Article

Liangxue-Qushi-Zhiyang Decoction Ameliorates DNCB-Induced Atopic Dermatitis in Mice through the MAPK Signaling Pathway Based on Network Pharmacology

Lili Zhang,[§] Huili Zhang,[§] Xiaoyu Niu, Xuan Zhang, Xingtong Chen, Shengyi Lei, Shengnan Ma, and Zhanxue Sun*

Cite This: *ACS Omega* 2024, 9, 17931−17944

Read Online

ACCESS | Metrics & More | Article Recommendations | Supporting Information

ABSTRACT: The traditional prescription of Liangxue-Qushi-Zhiyang decoction (LQZ) has been demonstrated to be efficacious in treating atopic dermatitis (AD), a chronic inflammatory skin disorder marked by intense itching, redness, rashes, and skin thickening. Nevertheless, there has been an inadequate systematic exploration of the potential targets, biological processes, and pathways for AD treatment through LQZ. The study objective was to evaluate the efficacy and possible mechanism of LQZ in AD mice. In our study, we identified the primary compounds of LQZ, analyzed hub targets, and constructed a network. Subsequently, the predicted mechanisms of LQZ in AD were experimentally studied and validated in vivo, as determined by network pharmacological analysis. A total of 80 serum components of LQZ were identified through ultra-performance liquid chromatography-electrospray ionization-tandem mass spectrometry (UPLC-ESI-MS/MS), among which 49 compounds were absorbed into the bloodstream. Our results indicated that LQZ targets six putative key factors in the MAPK signaling pathway, which play essential roles in AD, namely, EGFR, p-MAPK1/3, p-MAPK14, IL-1β, IL-6, and TNF-α. We observed spleen coefficient, dermatitis scores, and ear thickness were all downregulated in 2,4-dinitrochlorobenzene (DNCB)-induced mice after LQZ treatment. Histological analysis of the dorsal and ear skin further revealed that LQZ significantly decreased skin inflammation, epidermal thickness, and mast cell numbers compared to the DNCB group. Our study demonstrated the effectiveness of LQZ in reducing epidermal and dermal damage in a mouse model of AD. Furthermore, our findings suggest that downregulating the MAPK signaling pathway could be a potential therapeutic strategy for the treatment of AD.
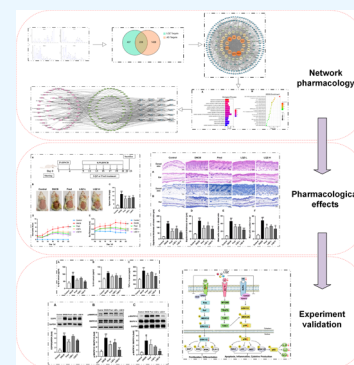
1. INTRODUCTION

Atopic dermatitis (AD) is a common chronic inflammatory skin disorder that manifests with symptoms such as dry skin, intense itching, and erythematous skin lesions.[1] It affects approximately 20% of children and 5−10% of adults globally, making it a worldwide health issue and one of the leading causes of nonfatal diseases.[2−4] The pathogenesis of AD is complex, involving both genetic and environmental factors.[5] It is believed that a disruption in the skin barrier leads to enhanced allergen penetration and increased colonization of the skin by *Staphylococcus aureus*.[3,6] Langerhans cells, inflammatory dendritic epidermal cells, and dermal dendritic cells receive allergens and irritants in lesional skin and release proinflammatory factors such as IL-1β and IL-33, which further stimulate type 2 skin lymphocytes (TH2 cells).[7,8] In turn, TH2 cells release IL-4, IL-13, and IL-31, activating cutaneous sensory nerves and causing itching in the body.[8] In AD therapy, anti-inflammatory therapy with topical corticosteroids or topical calcineurin inhibitors is a major element and represents the most effective and first-line treatment for reducing inflammation.[9] However, these topical treatments are associated with long-term use side effects, including skin atrophy, dermatoglyphia, telangiectasia, pigmentation, and stabbing pain.[10,11] Dry skin is a frequent clinical complication associated with numerous skin diseases, including psoriasis and atopic dermatitis (AD), as well as various systemic diseases.[12] Therefore, the application of moisturizers plays an indispensable role in the management of AD. For patients with moderate to severe AD, a combination of systemic treatments is often necessary, encompassing corticosteroids, immunosuppressants, and biologics.[13] Nonetheless, there are prevailing uncertainties regarding long-term management and treatment strategies for AD, especially concerning the long-term safety and efficacy of systemic treatments and emerging therapies.[14] Given these considerations, exploring treatments from Chinese medicine might present a viable alternative option for AD management.
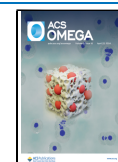
Table 1. Composition of LQZ

| Chinese pinyin name	latin name	species and genera	medicinal part	dosage (g)
Shuiniujiao	Bubali Cornu	*Bubalus bubalis* Linnaeus	horn	30
Shengdi	Rehmanniae Radix	*Rehmannia glutinosa* Libosch.	rhizome	15
Kushen	Sophorae Flavescentis Radix	*Sophora flavescens* Ait.	root	10
Chishao	Paeoniae Radix Rubra	*Paeonia lactiflora* Pall.	root	12
Shengyizhiren	Coicis Semen	*Coix lacryma-jobi* L.var.mayuen (Roman.) Stapf	seed	30
Baimaogen	Imperatae Rhizoma	*Imperata cylindrica* Beauv.var.major (Nees) C.E.Hubb.	rhizome	30
Zelan	Lycopi Herba	*Lycopus lucidus* Turcz.var.hirtus Regel	herb	10
Difuzi	Kochiae Fructus	*Kochia scoparia* (L.) Schrad.	fruit	15
Mudanpi	Moutan Cortex	*Paeonia suffruticosa* Andr.	cortex	12
Fuling	Poria	*Poria cocos* (Schw.) Wolf	sclerotium	15
Gancao	Glycyrrhizae Radix Et Rhizoma	*Glycyrrhiza uralensis* Fisch.	radix and rhizome	6
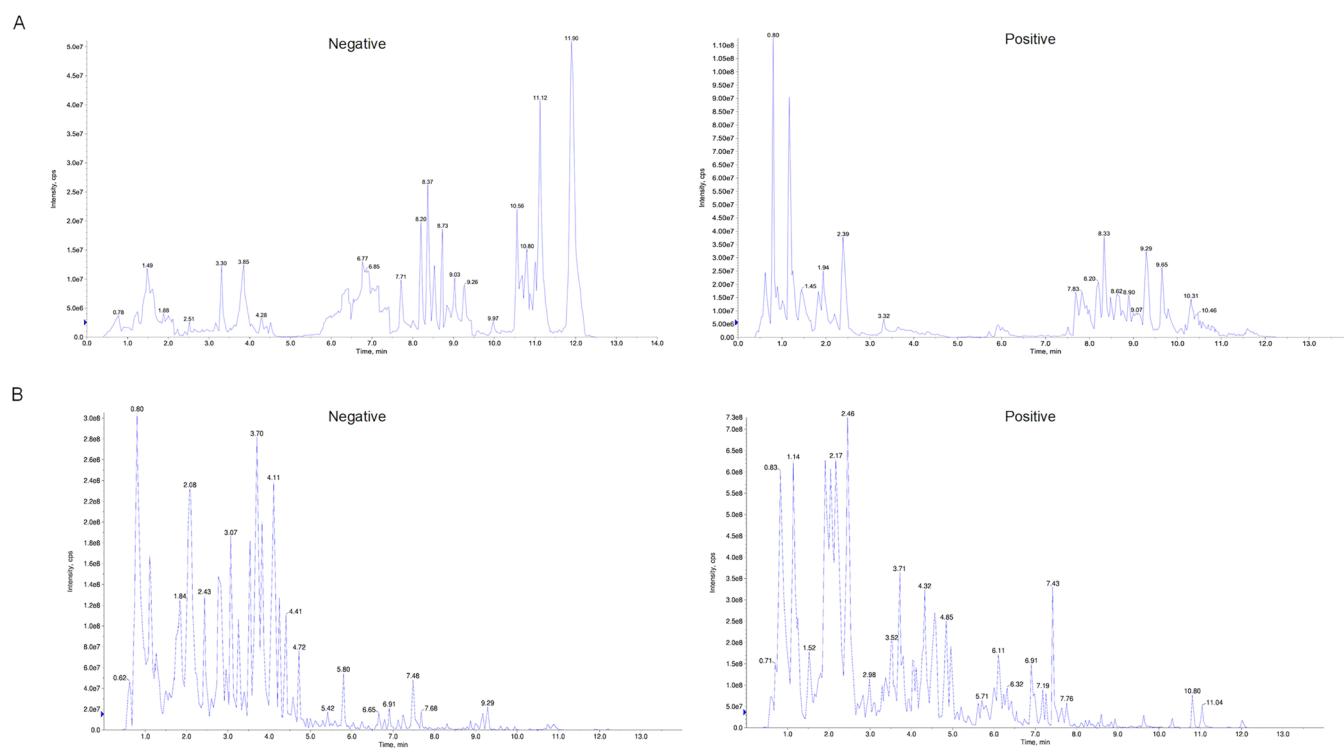
Figure 1. Total ion chromatogram monitored in negative and positive ion modes for (A) LQZ serum and (B) LQZ aqueous extract.

Liangxue-Qushi-Zhiyang decoction (LQZ), a classical traditional Chinese medicine formulation used for treating AD, consists of 11 different traditional Chinese medicinal herbs. The specific composition of the LQZ is detailed in Table 1. LQZ has been clinically used to treat AD, resulting in good outcomes and a relatively low recurrence rate.[15] Previous studies also confirmed that LQZ could control erythema, eliminate edema, repair the damaged epidermis, inhibit lichenification in a mouse model of AD. Sun found that, concurrently, serum IL-2 concentrations can be augmented and serum IL-4 and leukotriene B4 concentrations of lesions can be reduced.[16] Despite these findings, the in vivo metabolic components of LQZ and its exact mechanism of action in AD treatment remain elusive. Liquid chromatography with tandem mass spectrometry (LC-MS/MS) is a powerful analytical technique that combines the separating power of liquid chromatography with the highly sensitive and selective mass analysis capability of triple quadrupole mass spectrometry. It is extensively utilized in the analysis of traditional Chinese and Western medicines, their metabolic components, and endog-

enous substances in the body.[17] Numerous natural plant-derived compounds, including quercetin,[18] matrine,[19] and ononin,[20] have been proven to have strong potential in the management of skin diseases.

Network pharmacology coupled with systems biology can be utilized to effectively investigate the various kinds of components, objectives, and pathways of traditional Chinese medicine (TCM).[21] The application of integrative pharmacology can reveal the intricate molecular mechanisms that underlie TCM and establish new therapeutic applications beyond traditional TCM therapies.[22,23]

Our study aims to explore the therapeutic effects of LQZ on AD by utilizing ultra-performance liquid chromatography-electrospray ionization-MS/MS (UPLC-ESI-MS/MS) to identify the major ingredients of LQZ and conducting comprehensive network pharmacology analysis. Furthermore, we validated the proposed key targets of LQZ on 2,4-dinitrochlorobenzene-(DNCB)-induced AD in a mouse model.

Table 2. Identified Serum Compounds of LQZ by UPLC-MS/MS

no.	RT (min)	Q1 (Da)	molecular weight (Da)	formula	ionization model	compounds	class	CAS
1*	10.69	309.2	310.2144	$C_{18}H_{30}O_4$	$[M-H]^-$	13(s)-hydroperoxy-(9z,11e,15z)-octadecatrienoic acid	lipids	67597−26-6
2*	1.93	249.2	248.1889	$C_{15}H_{24}N_2O$	$[M+H]^+$	matrine	alkaloids	519-02-8
3	1.38	117.0193	118.0266	$C_4H_6O_4$	$[M-H]^-$	succinic acid	organic acids	110-15-6
4*	1.19	130.05	129.0426	$C_5H_7NO_3$	$[M+H]^+$	pyroglutamic acid	amino acids and derivatives	4042-36-8
5	0.81	130.09	129.079	$C_6H_{11}NO_2$	$[M+H]^+$	cycloleucine	amino acids and derivatives	52-52-8
6	0.9	118.09	117.079	$C_5H_{11}NO_2$	$[M+H]^+$	L-valine	amino acids and derivatives	72-18-4
7*	1.29	132.1	131.0946	$C_6H_{13}NO_2$	$[M+H]^+$	L-leucine	amino acids and derivatives	61-90-5
8*	0.81	175.12	174.1117	$C_6H_{14}N_4O_2$	$[M+H]^+$	L-arginine	amino acids and derivatives	74-79-3
9*	1.29	132.1	131.0946	$C_6H_{13}NO_2$	$[M+H]^+$	L-norleucine	amino acids and derivatives	327-57-1
10	1.49	267.07	268.0808	$C_{10}H_{12}N_4O_5$	$[M-H]^-$	9-(arabinosyl)hypoxanthine	nucleotides and derivatives	7013-16-3
11	1.54	123.06	122.048	$C_6H_6N_2O$	$[M+H]^+$	nicotinamide	others	98−92-0
12	0.77	118.09	117.079	$C_5H_{11}NO_2$	$[M+H]^+$	betaine	alkaloids	107-43-7
13	1.99	249.2	248.1889	$C_{15}H_{24}N_2O$	$[M+H]^+$	isomatrine	alkaloids	17801-36-4
14*	1.98	166.09	165.079	$C_9H_{11}NO_2$	$[M+H]^+$	L-phenylalanine	amino acids and derivatives	63-91-2
15	2.18	221.09	220.0848	$C_{11}H_{12}N_2O_3$	$[M+H]^+$	5-hydroxy-DL-tryptophan(5-HTP)	amino acids and derivatives	56-69-9
16*	2.22	220.12	219.1107	$C_9H_{17}NO_5$	$[M+H]^+$	D-pantothenic acid	others	79-83-4
17	2.48	118.07	117.0578	C_8H_7N	$[M+H]^+$	indole	alkaloids	120-72-9
18*	1.19	130.09	129.079	$C_6H_{11}NO_2$	$[M+H]^+$	L-pipecolic acid	organic acids	3105-95-1
19*	2.41	146.06	145.0528	C_9H_7NO	$[M+H]^+$	8-hydroxyquinoline	alkaloids	148-24-3
20	2.41	130.06	129.0578	C_9H_7N	$[M+H]^+$	isoquinoline	alkaloids	119-65-3
21*	4.53	187.1	188.1049	$C_9H_{16}O_4$	$[M-H]^-$	azelaic acid	organic acids	123-99-9
22*	2	247.18	246.1732	$C_{15}H_{22}N_2O$	$[M+H]^+$	sophocarpine	alkaloids	145572−44-7
23*	1.2	151.03	152.0334	$C_5H_4N_4O_2$	$[M-H]^-$	xanthine	nucleotides and derivatives	69-89-6
24*	1.19	182.08	181.0739	$C_9H_{11}NO_3$	$[M+H]^+$	N-(2-hydroxy-4-methoxyphenyl)acetamide	alkaloids	58469-06-0
25*	1.9	283.07	284.0757	$C_{10}H_{12}N_4O_6$	$[M-H]^-$	xanthosine	nucleotides and derivatives	146-80-5
26	3.32	377.15	376.1383	$C_{17}H_{20}N_4O_6$	$[M+H]^+$	riboflavin (vitamin B2)	others	83-88-5
27*	1.91	268.1	267.0968	$C_{10}H_{13}N_5O_4$	$[M+H]^+$	adenosine	nucleotides and derivatives	58-61-7
28*	2.38	205.1	204.0899	$C_{11}H_{12}N_2O_2$	$[M+H]^+$	cyclo-(gly-phe)	amino acids and derivatives	10125-07-2
29	3.39	359.13	358.1264	$C_{16}H_{22}O_9$	$[M+H]^+$	sweroside	terpenoids	14215-86-2
30*	3.94	163.04	164.0473	$C_9H_8O_3$	$[M-H]^-$	2-hydroxycinnamic acid	phenolic acids	583-17-5
31*	2.44	203.08	204.0899	$C_{11}H_{12}N_2O_2$	$[M-H]^-$	L-tryptophan	amino acids and derivatives	73-22-3
32*	3.94	163.04	164.0473	$C_9H_8O_3$	$[M-H]^-$	α-hydroxycinnamic acid	phenolic acids	5801-57-0
33	1.41	265.19	264.1838	$C_{15}H_{24}N_2O_2$	$[M+H]^+$	sophoranol	alkaloids	3411-37-8
34*	0.81	527.16	504.169	$C_{18}H_{32}O_{16}$	$[M+Na]^+$	maltotriose	others	1109-28-0
35*	3.17	137.02	138.0317	$C_7H_6O_3$	$[M-H]^-$	protocatechualdehyde	others	139-85-5
36*	2.13	384.12	383.1077	$C_{14}H_{17}N_5O_8$	$[M+H]^+$	succinyladenosine	nucleotides and derivatives	4542-23-8
37*	10.62	271.23	272.2351	$C_{16}H_{32}O_3$	$[M-H]^-$	2-hydroxyhexadecanoic acid	organic acids	764-67-0
38*	3.17	137.02	138.0317	$C_7H_6O_3$	$[M-H]^-$	2,5-dihydroxybenzaldehyde	others	1194-98-5
39*	8.25	285.21	286.2144	$C_{16}H_{30}O_4$	$[M-H]^-$	hexadecanedioic acid	lipids	505-54-4
40*	1.19	182.08	181.0739	$C_9H_{11}NO_3$	$[M+H]^+$	3-hydroxy-L-phenylalanine	amino acids and derivatives	587-33-7
41*	8.91	295.23	296.2351	$C_{18}H_{32}O_3$	$[M-H]^-$	13(S)-hydroxyoctadeca-9Z,11E-dienoic acid	lipids	10219-69-9
42*	8.91	295.23	296.2351	$C_{18}H_{32}O_3$	$[M-H]^-$	9S-hydroxy-10E,12Z-octadecadienoic acid	lipids	15514-85-9
43*	8.91	295.23	296.2351	$C_{18}H_{32}O_3$	$[M-H]^-$	α-hydroxylinoleic acid	lipids	57818-44-7
44	3.98	503.12	502.1111	$C_{24}H_{22}O_{12}$	$[M+H]^+$	6″-O-malonyldaidzin	flavonoids	124590-31-4
45*	3.34	179.03	180.0423	$C_9H_8O_4$	$[M-H]^-$	caffeic acid	phenolic acids	331-39-5
46*	1.19	182.08	181.0739	$C_9H_{11}NO_3$	$[M+H]^+$	L-tyrosine	amino acids and derivatives	60-18-4
47*	4.03	447.09	446.0849	$C_{21}H_{18}O_{11}$	$[M+H]^+$	apigenin-7-O-glucuronide	flavonoids	29741-09-1
48	0.79	179.06	180.0634	$C_6H_{12}O_6$	$[M-H]^-$	L-glucose	others	921-60-8
49	0.79	179.0556	180.0634	$C_6H_{12}O_6$	$[M-H]^-$	sorbose	others	3615-56-3

Table 2. continued

no.	RT (min)	Q1 (Da)	molecular weight (Da)	formula	ionization model	compounds	class	CAS
50*	0.79	179.05	180.0634	$C_6H_{12}O_6$	$[M-H]^-$	inositol	others	87-89-8
51*	4.37	563.18	562.1686	$C_{27}H_{30}O_{13}$	$[M+H]^+$	glycyroside	flavonoids	125310-04-5
52	4.37	563.17	562.1686	$C_{27}H_{30}O_{13}$	$[M+H]^+$	kushenol O	flavonoids	102390-91-0
53	2.38	188.0706	187.0633	$C_{11}H_9NO_2$	$[M+H]^+$	3-indoleacrylic acid	alkaloids	1204-06-4
54*	3.94	211.14	210.1368	$C_{11}H_{18}N_2O_2$	$[M+H]^+$	cyclo(D-leu-L-pro)	amino acids and derivatives	36238-67-2
55	10.87	301.22	302.2246	$C_{20}H_{30}O_2$	$[M-H]^-$	pimaric acid	terpenoids	127-27-5
56	3.87	193.05	194.0579	$C_{10}H_{10}O_4$	$[M-H]^-$	ferulic acid	phenolic acids	537-98-4
57*	3.92	165.05	164.0473	$C_9H_8O_3$	$[M+H]^+$	caffeic aldehyde	phenolic acids	141632-15-7
58*	3.94	211.13	210.1368	$C_{11}H_{18}N_2O_2$	$[M+H]^+$	cyclo(pro-leu)	amino acids and derivatives	5654-86-4
59*	2.66	219.11	218.1055	$C_{12}H_{14}N_2O_2$	$[M+H]^+$	N-formylcytisine	alkaloids	53007-06-0
60	11.7	255.23	256.2402	$C_{16}H_{32}O_2$	$[M-H]^-$	palmitic acid	lipids	57-10-3
61	2.77	183.03	184.0372	$C_8H_8O_5$	$[M-H]^-$	3-O-methylgallic acid	phenolic acids	3934-84-7
62	1.88	245.16	244.1576	$C_{15}H_{20}N_2O$	$[M+H]^+$	rhombifoline	alkaloids	529-78-2
63	5.27	331.04	330.0376	$C_{16}H_{10}O_8$	$[M+H]^+$	3,3′-O-dimethylellagic acid	tannins	2239-88-5
64	1.98	281.19	280.1787	$C_{15}H_{24}N_2O_3$	$[M+H]^+$	5,9-dihydroxymatrine	alkaloids	72362-00-6
65*	4.05	165.06	166.063	$C_9H_{10}O_3$	$[M-H]^-$	DL-3-phenyllactic acid	organic acids	828-01-3
66*	4.07	165.06	166.063	$C_9H_{10}O_3$	$[M-H]^-$	2,6-dimethoxybenzaldehyde	others	3392–97-0
67*	2.96	495.15	496.1581	$C_{23}H_{28}O_{12}$	$[M-H]^-$	oxypaeoniflorin	terpenoids	39011-91-1
68	4.08	165.06	166.063	$C_9H_{10}O_3$	$[M-H]^-$	3-(3-hydroxyphenyl)-propionic acid	phenolic acids	621-54-5
69*	3.92	165.05	164.0473	$C_9H_8O_3$	$[M+H]^+$	p-coumaric acid	phenolic acids	501-98-4
70	8.74	317.21	318.2195	$C_{20}H_{30}O_3$	$[M-H]^-$	12-hydroxy-5,8,10,14,17-eicosapentaenoic acid	lipids	81187-21-5
71*	5.66	215.13	216.1362	$C_{11}H_{20}O_4$	$[M-H]^-$	undecanedioic acid	lipids	1852-04-6
72	3.99	206.08	207.0895	$C_{11}H_{13}NO_3$	$[M-H]^-$	N-acetyl-L-phenylalanine	amino acids and derivatives	2018-61−3
73*	4.68	431.13	430.1264	$C_{22}H_{22}O_9$	$[M+H]^+$	formononetin-7-O-glucoside (ononin)	flavonoids	486-62-4
74	11.07	282.28	281.2719	$C_{18}H_{35}NO$	$[M+H]^+$	oleamide (9-octadecenamide)	lipids	301-02-0
75	5.92	329.2334	330.2406	$C_{18}H_{34}O_5$	$[M-H]^-$	9,10,13-trihydroxy-11-octadecenoic acid	lipids	29907-57-1
76*	1.65	183.03	184.0372	$C_8H_8O_5$	$[M-H]^-$	methyl gallate	phenolic acids	99-24-1
77*	9.69	295.23	296.2351	$C_{18}H_{32}O_3$	$[M-H]^-$	12,13-epoxy-9-octadecenoic acid	lipids	6799-85-5
78*	2.33	359.1	360.1056	$C_{15}H_{20}O_{10}$	$[M-H]^-$	glucosyringic acid	phenolic acids	33228-65-8
79*	4.03	165.06	166.063	$C_9H_{10}O_3$	$[M-H]^-$	2-hydroxy-3-phenylpropanoic acid	phenolic acids	7326-19-4
80	9.74	295.23	296.2351	$C_{18}H_{32}O_3$	$[M-H]^-$	(9R,10S)-(12Z)-9,10-epoxyoctadecenoic acid	lipids	16833-56-0

2. RESULTS

2.1. UPLC-ESI-MS/MS Analysis Identified Ingredients in the LQZ. UPLC-ESI-MS/MS was employed to analyze the chemical components of LQZ in serum and water extracts (Figure 1). We identified 310 metabolites in the LQZ solution (Total Ion Chromatogram shown in Figure 1B and Table S1). Post oral administration of this compound formula at a dose of 7.6 g/kg to healthy mice, blood samples were collected to identify the compounds absorbed into the serum. We detected 80 metabolites in the LQZ serum samples (Total Ion Chromatogram shown in Figure 1A and Table 2), including 15 amino acids and derivatives, 13 alkaloids, 12 lipids, 11 phenolic acids, 5 flavonoids, 5 organic acids, 5 nucleotides and derivatives, 3 terpenoids, 1 tannin, and 10 other compounds. Comparison of the retention time (t_R) values and MS fragment characteristics between the compounds in the LQZ serum and extracts revealed 49 compounds in both, considered to be absorbed into the bloodstream.[24] These include 11 amino acids and their derivatives, 8 phenolic acids, 7 lipids, 5 alkaloids, 4 organic acids, 4 nucleotides and their derivatives, 3 flavonoids, 1 terpenoid, and 6 others. Table 2 provides detailed identification information for LQZ serum compounds, including retention time ((RT) (min)), parent ion molecular weight postionization by the electrospray ion source (Q1 (Da)), molecular weight (Da), molecular formula (Formula), ionization model ((M + H for positive, M − H for negative)), compound name (Compounds), first-level category (Class), and CAS number (CAS).

2.2. Acquisition of Putative Targets between Compounds and AD. Based on the information in Table 2, 49 compounds from LQZ were absorbed into the bloodstream of mice, indicating their potential role as key components in LQZ.[25] These compounds are predominantly amino acids and their derivatives, alkaloids, lipids, and phenolic compounds. After eliminating redundant data, we identified 665 potential targets related to LQZ using the SwissTargetPrediction database. The interactions among these 49 compounds and their potential targets are detailed in Table S3.

Additionally, we sourced 1667 recognized therapeutic targets for AD from the GeneCards database. As depicted in Figure 2, there are 228 overlapping targets between the
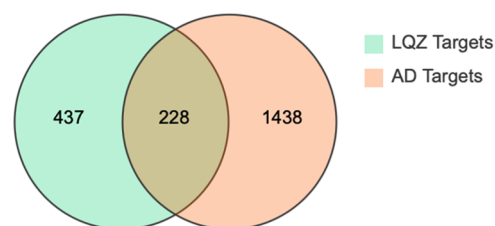
Figure 2. Potential overlapping targets for LQZ and AD.
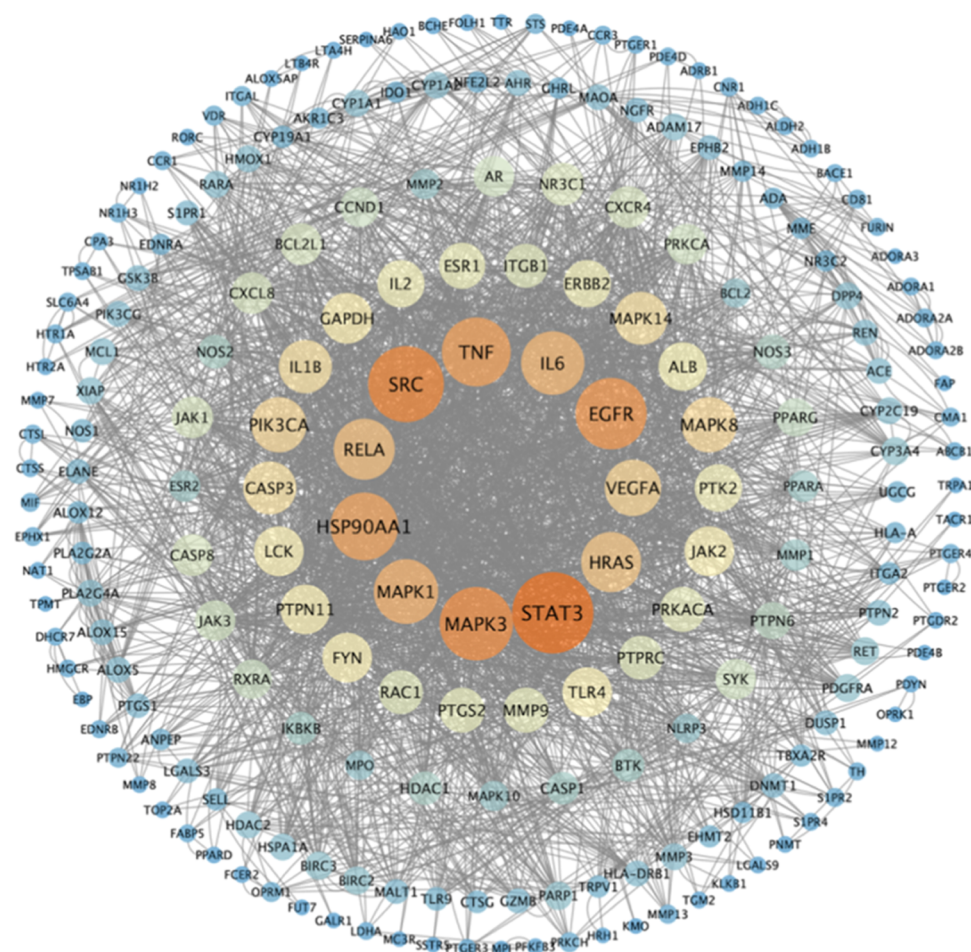
Figure 3. Protein−protein Interaction (PPI) network of related targets for LQZ in the treatment of AD. As the degree of targets increased, the circle became larger, and the color changed from orange to blue.
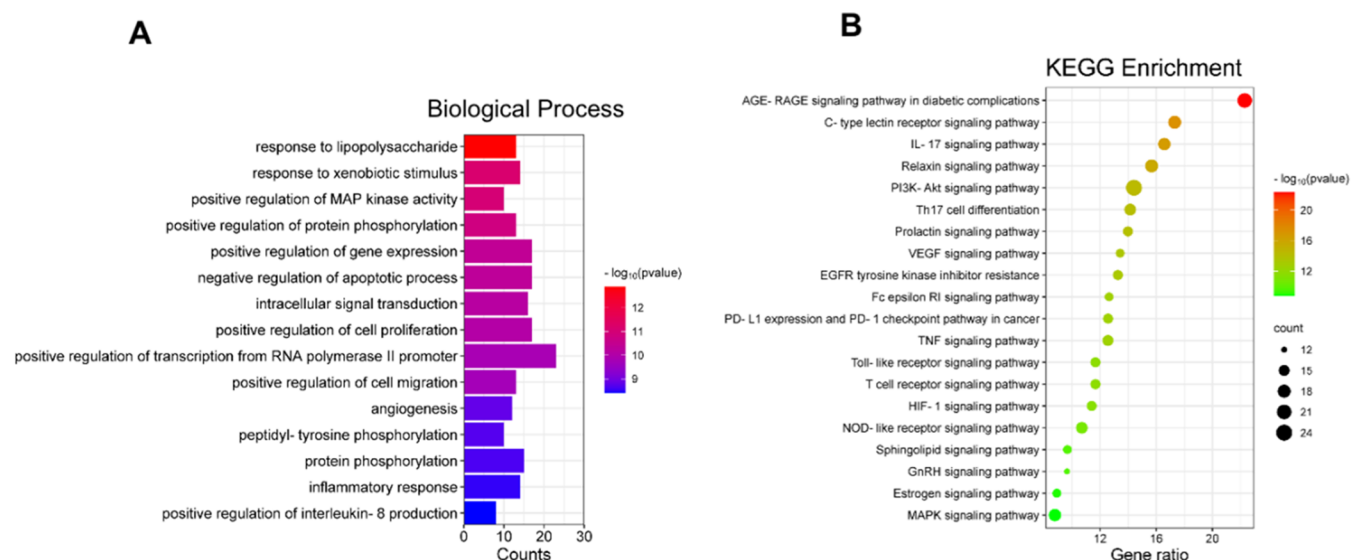
Figure 4. (A) GO and (B) KEGG enrichment.

potential targets of LQZ and the known therapeutic targets for AD. This overlap suggests that these points are critical targets for LQZ in the treatment of AD.

2.3. Construction of the PPI Network. The PPI network was constructed using the STRING 11.5 database and

visualized with Cytoscape 3.9.1, after excluding disconnected nodes. The resulting network contained 209 nodes and 2494 edges (Figure 3). A thorough overview of 209 potential targets was furnished in Table S4. To further investigate the interaction between the 209 target proteins, we analyzed

Figure 5. Compound−target−pathway network of identified key compounds, key targets, and the top 20 pathways using the KEGG database. Pink ellipse nodes represent the compounds in LQZ, green diamond nodes represent the key targets, and blue "V" represent the pathways enriched according to the KEGG database.

Figure 6. Effects of LQZ on the spleen coefficient, dermatitis scores, and ear thickness of the DNCB-treated mice. (A) Experimental scheme for the DNCB-induced AD-like mouse model. (B) LQZ-treated mice are protected against DNCB-induced AD-like skin lesions in mice. (C) Spleen coefficient, (D) dermatitis scores, and (E) ear thickness in each group. Data were expressed as mean ± SD (nTOC = 6), versus the control group, $^{\#\#\#}p < 0.001$, versus the DNCB group, $^{**}p < 0.01$, $^{***}p < 0.001$.

Figure 7. Effects of LQZ on histopathologic findings. (A) Representative photos of the histopathological features of the dorsal and ear skin with H&E staining (×200). The black straight line indicates epidermal thickness. (B) Representative photos of the mast cells infiltration in the dorsal and ear skin with toluidine blue staining (×200). The arrows indicate mast cells. Statistical analysis of epidermal thickness of (C) dorsal and (D) ear skin. Statistical analysis of mast cell numbers in (E) dorsal and (F) ear skin. Data were expressed as mean ± SD ($n = 3$), versus the control group, $^{###}p < 0.001$, versus the DNCB group, $^{*}p < 0.05$, $^{**}p < 0.01$, $^{***}p < 0.001$.

three topological features of the Cytoscape network: betweenness centrality, closeness centrality, and degree above the median. Table S5 identified 71 targets that met the criteria of betweenness centrality > 0.00216, closeness centrality > 0.3502, and degree > 14, indicating them as the primary targets of LQZ against AD. Figure 3 illustrates the immune and inflammatory responses in the PPI network, which were identified using gene annotation. The findings indicate that LQZ exhibits potential pharmacological effects in combating infection, inflammation, and organism-related impairments.

2.4. GO Analyses and KEGG Enrichment. The top 15 GO terms with the most representative from the GO enrichment analysis (adjusted $p < 0.01$) are shown in Figure 4A. Inflammatory response, response to lipopolysaccharide, xenobiotic stimulus, MAP kinase activity, protein phosphorylation, and intracellular signal transduction, the primary biological process associated with the targets, were significantly regulated.

A total of 167 KEGG pathways, with an adjusted p-value of less than 0.01, were identified as being of great significance. Figure 4B illustrates the top 20 KEGG pathways after excluding human disease pathways. The MAPK signaling pathway was enriched with important targets for immune and inflammatory responses, including EGFR, MAPK1, MAPK3, MAPK14, IL-1β, IL-6, and TNF-α. The activation of the MAPK signaling pathway is known to be pivotal in the generation of proinflammatory cytokines, such as TNF, IL-1, and IL-6.[26]

2.5. Compound−Target−Pathway Network Analysis. In our study, we identified 49 compounds from LQZ that were absorbed into the bloodstream. These compounds are linked to 71 key targets for AD treatment and are involved in the top 20 related pathways (Figure 5). Utilizing Cytoscape 3.7.1, we developed a network model to illustrate the compound−target−pathway interactions. The 49 components absorbed from LQZ comprise 11 amino acids and their derivatives, 8 phenolic acids, 7 lipids, 5 alkaloids, 4 organic acids, 4 nucleotides and their derivatives, 3 flavonoids, 1 terpenoid, and 6 other compounds. Predominantly, these fall into four categories: amino acids and their derivatives (e.g., L-arginine and L-phenylalanine), alkaloids (e.g., Matrine and Sophocarpine), lipids (e.g., α-hydroxylinoleic acid), and phenolic compounds (e.g., caffeic acid). Critical targets in immune and inflammatory responses, including IL-1, IL-6, TNF, EGFR, MAPK1, MAPK3, and MAPK14, are largely found in the MAPK signaling pathway. This insight is crucial to understanding the potential mechanisms by which LQZ could treat AD.

2.6. LQZ Alleviated DNCB-Induced AD. The DNCB group's dorsal skin, as depicted in Figure 6B, was subject to AD-like lesions, including erythema, edema, excoriations, and dryness, after multiple applications of the drug. However, an apparent recovery of skin lesions could be observed in the LQZ-treated and Pred-treated groups compared with the DNCB mice. A significant increase in the spleen index was observed in DNCB-treated mice compared with the control group. However, LQZ treatment was found to reverse this
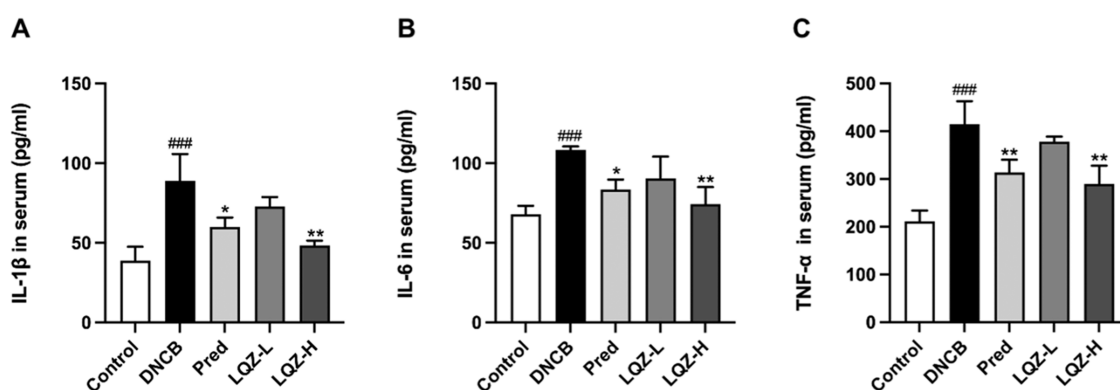
Figure 8. Serum levels of (A) IL-1β, (B) IL-6, and (C) TNF-α in the different groups, as measured using an ELISA. Data were expressed as mean $\pm$ SD ($n = 3$), versus the control group, $^{\#\#\#}p < 0.001$, versus the DNCB group, $^{*}p < 0.05$, $^{**}p < 0.01$.
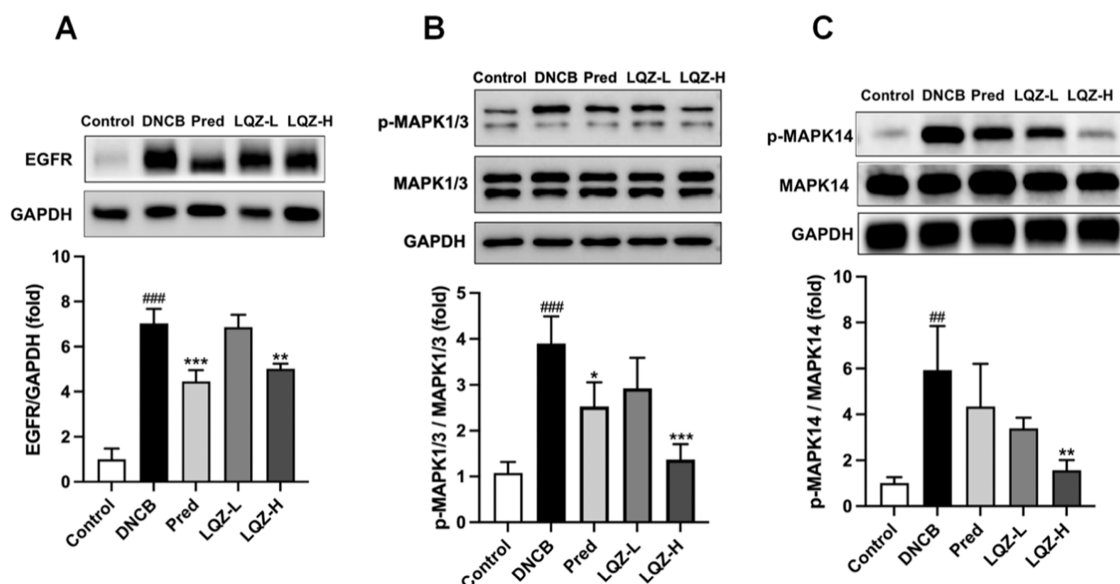
Figure 9. Protein levels of (A) EGFR, (B) p-MAPK1/3, and (C) p-MAPK14 in different groups, as measured using Western blotting. Data were expressed as mean $\pm$ SD ($n = 3$), versus the control group, $^{\#\#}p < 0.01$, $^{\#\#\#\#}p < 0.001$, versus the DNCB group, $^{*}p < 0.05$, $^{**}p < 0.01$, $^{***}p < 0.001$.

increase (Figure 6C). Based on the clinical severity of AD-like symptoms, administration of high-dose LQZ, low-dose LQZ, and Pred significantly reduced the clinical score as compared to the model mice (Figure 6D). Meanwhile, the scores of AD-like skin lesions in mice saw an improvement in a dose-dependent manner when LQZ was administered during the same period. Figure 6B,E depicts that, in comparison with healthy mice, the mice repeatedly exposed to DNCB had red and swollen ears. Treating with LQZ or Pred relieved the redness in the ears. The DNCB group's ears showed a remarkable augmentation, in contrast to the LQZ-treated or Pred-treated groups, which had a considerable diminishment in ear thickness. These results showed that LQZ could symptomatically relieve DNCB-induced AD in mice efficaciously.

2.7. Histopathologic Alterations of DNCB-Induced Mice in the Wake of LQZ. A histological analysis of the mice treated with DNCB revealed a noteworthy epidermal thickening of their back skin and ear tissue, with a 6.9-fold augmentation of the back skin and 3.6-fold augmentation of the ear tissue compared to the normal mice. Oral administration of LQZ-H (15.2 g/kg) caused a reduction in thickness on the dorsal and ear skin by 58.3 and 45.1%,

respectively, as compared with the DNCB group. Prednisolone treatment also showed a considerable reduction in epidermal thickening of the dorsal and ear skin when compared to the model mice, with a reduction of 49.6% in the dorsal skin and 39.6% in the ear skin (Figure 7A,C,D). Our data demonstrated that the LQZ-H group showed a similar reduction in epidermal thickening of the dorsal skin and ear when compared to the Pred group.

To further investigate the effects of LQZ on mast cell infiltration, dorsal and ear skin sections were stained with toluidine blue. The number of mastocytes was found to be significantly increased by 6.0- and 4.7-fold in the back and ear skin, respectively, when compared to the control group. However, LQZ-H treatment was found to significantly suppress the proliferation of mast cells by 48.9% in the dorsal skin and 45.2% in the ears, when compared to the DNCB group. Additionally, Pred treatment also significantly reduced the infiltrated mastocyte in the dorsal and ear skin by 30.9 and 39.7%, respectively, as compared with the DNCB group (Figure 7B,E,F). Notably, LQZ-H treatment showed a superior inhibitory effect on the infiltration of mastocytes in the dorsal and ear skin of the sensitized mice when compared to the positive control.
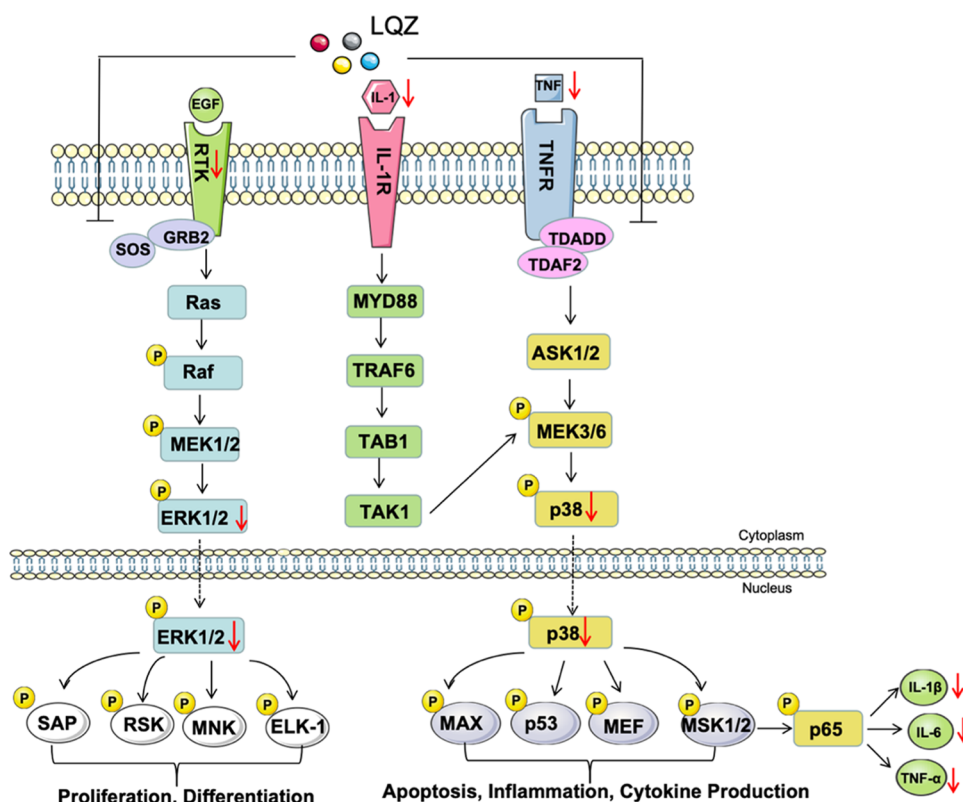
Figure 10. Modulating the MAPK signaling pathway of LQZ against AD. EGF, IL-1, and TNF initiate a series of kinase activations through their respective cell surface receptors in the MAPK pathway: EGFR (RTK), IL-1R, and TNFR. These activations lead to the activation of p-MAPK3/1 (p-ERK1/2) and p-MAPK14 (p38), which, in turn, activate p65. This regulates the release of inflammatory factors such as IL-1β, IL-6, and TNF-α, influencing cellular processes such as proliferation, differentiation, apoptosis, inflammatory responses, and cytokine production. The therapeutic effect of LQZ-H on AD potentially involves reducing the expressions of EGFR, p-MAPK1/3, p-MAPK14, IL-1β, IL-6, and TNF-α, thus inhibiting the MAPK pathway.

2.8. LQZ Decreases the Levels of IL-1β, IL-6, and TNF-α in Serum. Analysis of network pharmacology revealed that LQZ's action in treating atopic dermatitis may be linked to the reaction to xenobiotic stimulus and inflammatory reaction. As illustrated in Figure 8, the serum of mice after DNCB induction had a marked increase in IL-1β, IL-6, and TNF-α, yet this was remarkably reduced upon the LQZ-H group, in contrast to the model group. No noteworthy disparities in serum IL-1β, IL-6, and TNF-α concentrations were observed between the LQZ-L treatment group and the model group; However, the LQZ-L treatment did demonstrate a tendency to suppress serum IL-1β, IL-6, and TNF-α concentrations. These findings demonstrated that LQZ could abate the inflammatory response in the serum of DNCB-induced mice.

2.9. LQZ Inhibits the MAPK Signaling Pathway. To verify the reliability of the network pharmacology prediction results, Western blotting was used to measure the expression of EGFR, p-MAPK1/3, MAPK1/3, p-MAPK14, and MAPK14 in AD mice. Compared with the control group, DNCB induced a significant increase in the expression of these proteins in the skin tissue of mice (Figure 9). LQZ treatment could dose-dependently reduce the DNCB-induced upregulation of their expression (Figure 9). The MAPK signaling cascade is an evolutionarily conserved enzyme that connects cell surface receptors to key regulatory targets within cells. It has a wide range of physiological functions in controlling gene expression, cell proliferation, and programmed cell death.[27] EGFR, MAPK1/3, MAPK14, IL-1β, IL-6, and TNF-α (measured by

ELISA) are key targets involved in the MAPK signaling pathway. This suggests that LQZ may inhibit DNCB-induced mouse AD by inhibiting the MAPK signaling pathway.

3. DISCUSSION

AD is a common allergic and inflammatory skin disorder that leads to itching, recurrent eczematous lesions, erythema, dryness, and significantly impairs the quality of life.[28] Topical therapy is a common approach for alleviating clinical symptoms, but it can have the side effect of thinning and increasing sensitivity of the skin.[8] Hence, finding new and effective therapeutic agents for AD is necessary. LQZ, a drug that has been extensively studied for the treatment of AD, exhibits numerous beneficial characteristics and has shown proven efficacy in both clinical and experimental settings.[15,16] However, the specific pharmacologic mechanism of action of LQZ in treating AD remains incompletely understood.

In our study, an integrative pharmacology strategy was used to explore the effects and mechanisms of LQZ in treating AD. By UPLC-MS/MS (Figure 1) and network pharmacology analysis, 80 serum components of LQZ were identified. AD's pathological processes are strongly linked to inflammatory reaction and reaction to xenobiotic stimulus. Six potential targets of LQZ (EGFR, p-MAPK1/3, p-MAPK14, IL-1β, IL-6, and TNF-α) are essential elements in MAPK signaling pathways and are a major factor in AD (Figures 2−5). Subsequently, the potential mechanism of LQZ on AD predicted by network pharmacological analysis was exper-

imentally studied and verified in vivo. In comparison to the control group, the DNCB-treated mice exhibited an increase in the spleen coefficient, dermatitis scores, ear thickness, and skin histology (Figure 6) when we observed them. However, after administrating LQZ for a period of 14 days, the above results were all improved. Meanwhile, dorsal and ear skin histology showed LQZ treatments significantly decreased skin inflammation, epidermal thickness, and mastocyte numbers compared with the DNCB group (Figure 7). Our research demonstrated the effectiveness of LQZ treatments in reducing epidermal and dermal damage caused in a mouse model of atopic dermatitis. Additionally, through network pharmacology analysis, we discovered that the beneficial effects of LQZ are associated with the downregulation of MAPK signaling pathways (Figures 8 and 9). The main biological processes are listed in Figure 10.

In our UPLC-MS analysis, 310 compounds were identified in the LQZ solution. From the LQZ serum samples, we identified 80 compounds, of which 49 were absorbed into the bloodstream. These include 11 amino acids and their derivatives, 8 phenolic acids, 7 lipids, 5 alkaloids, 4 organic acids, 4 nucleotides and their derivatives, 3 flavonoids, 1 terpenoid, and 6 other compounds. The compounds that were absorbed into the bloodstream predominantly fall into four categories: amino acids and their derivatives (such as L-arginine and L-phenylalanine), alkaloids (such as Matrine and Sophocarpine), lipids (such as α-hydroxylinoleic acid), and phenolic compounds (such as caffeic acid). Chronic inflammation is the root cause of these atopic diseases. Matrine regulated Th1/Th2 inflammatory responses by inhibiting the Hsp90/NF-κB signaling axis to alleviate atopic dermatitis.[19] The Arg/NO pathway is activated in atopic diseases.[29] The anti-inflammatory mechanism exerted by L-arginine was to inhibit NF-κB activation via downregulating PI3K/Akt.[30] In RAW 264.7 cells induced by LPS, Wang discovered that sophocarpine had a suppression effect on the production of TNF-α, IL-1β, or IL-6,[31] while phenylalanine inhibited the production of IL-1β and TNF-α in proinflammatory (M1) macrophages.[32] α-Hydroxylinoleic acid, a metabolite of polyunsaturated fatty acids, has been identified to possess anti-inflammatory properties.[33,34] Caffeic acid, which was the main component of Qingxue jiedu formulation, inhibited the activations of STAT3, MAPK, and NF-κB signaling pathways and possessed a significant therapeutic effect on AD.[35] These findings suggested that LQZ attenuated skin damage by regulating inflammation and the immune process. While our study primarily focuses on the efficacy of traditional herbal medicine, we place equal importance on its safety. A thorough literature review was conducted on the 80 serum components found in LQZ, and we found no known toxic elements among these components. Moreover, previous clinical trials have established the safety of LQZ, with patients reporting positive therapeutic outcomes and no incidents of toxicity.[15] Even though the ingredients in the LQZ serum are deemed safe, we still advocate for the rational use of LQZ and the implementation of strict quality control measures. This approach is essential to ensure the safety of patients and the effectiveness of the treatment.

The KEGG enrichment analysis revealed that the MAPK signaling pathway may play a crucial role in AD. The main biological activities linked to these targets are the inflammatory response, response to xenobiotics, response to lipopolysaccharides, and positive regulation of MAP kinase activity.

Excessive inflammatory responses and impaired xenobiotic stimulus response play a crucial role in the pathogenesis of AD.[36] EGFR belongs to the receptor tyrosine kinase (RTK) family. When EGFR binds to specific ligands like EGF or TGF-α, it undergoes dimerization, leading to the activation of its intrinsic tyrosine kinase.[37] This activation initiates the stimulation of several downstream signaling pathways. Among them, the MAPK pathway, activated by EGF and EGFR signals, has been shown to control a wide range of physiological and pathological processes, including cell proliferation, gene expression, programmed cell death, and inflammation.[38] Prior research has suggested that diminishing the expression of EGFR within the MAPK pathway can effectively alleviate the symptoms of AD in mice.[39,40] MAPKs, including ERK1/2 (MAPK3/1), JNK1/2/3, and p38 proteins (MAPK14), have been reported to be involved in AD.[41−43] IL-1β1, IL-6, and TNF-α act as proinflammatory cytokine genes, which can be activated by MAPK signaling pathways.[44] Generally, an important cause of AD is the dysregulated Th1 and Th2 response.[45] Inflammation and immune responses in AD skin lesions are commonly regulated by proinflammatory cytokines, such as IL-4, IL-6, and IL-1.[46] In summary, blocking these proinflammatory factors may be the pharmacological mechanism of LQZ acting on AD. Using Western blotting or ELISA, we identified six targets (EGFR, p-MAPK1/3, p-MAPK14, IL-1β, IL-6, and TNF-α) associated with the MAPK signaling pathway in DNCB-induced mice. Our research uncovered noteworthy diminutions in the expressions of EGFR, p-MAPK1/3, p-MAPK14, IL-1β, IL-6, and TNF-α, implying that LQZ effectively hindered the MAPK signaling cycle.

Although we have shown the efficacy of LQZ in reducing the key protein of the MAPK pathway in animal models, cellular-level verification is still pending. We identified 49 compounds from LQZ that were absorbed into the bloodstream by using UPLC-MS/MS technology. However, the specific concentrations of these compounds in the blood are currently unknown. Therefore, future research should include in vivo pharmacokinetic studies to gain a deeper understanding of the efficacy and mechanisms of action of these compounds in the body.

4. CONCLUSIONS

In our investigation into the mechanism of action of LQZ on DNCB-induced AD, we utilized a blend of network pharmacology and experimental validation. The results from our research suggest that LQZ mitigates skin damage caused by DNCB in AD mice by downregulating the MAPK pathway. This recent discovery could potentially broaden the spectrum of treatment choices available to clinical doctors for patients with AD.

5. MATERIALS AND METHODS

5.1. Preparation of LQZ Serum and LQZ Solution. LQZ, provided by Dongfang Hospital of Beijing University of Chinese Medicine, is a compound of 11 herbs: *Bubali cornu* (30 g), *Rehmanniae radix* (15 g), *Sophorae flavescentis radix* (10 g), *Paeoniae radix rubra* (12 g), *Coicis semen* (30 g), *Imperatae rhizoma* (30 g), *Lycopi herba* (10 g), *Kochiae fructus* (15 g), *Moutan cortex* (12 g), *Poria* (15 g), and *Glycyrrhizae radix et rhizoma* (6 g). The composition details are given in Table 1. To prepare LQZ solution, 1850 g of the herbal mixture was

first soaked in water for 1 h and then boiled in 18,500 mL of distilled water for 30 min. The residue was filtered and the filtrate collected. The residue was then reboiled in 10,000 mL of distilled water for another 30 min, followed by filtration and collection of the second filtrate. These combined filtrates were concentrated via a rotary evaporator to produce a LQZ extract, which was freeze-dried and sterilized, resulting in a 20% extract. The used daily dosage of LQZ in mice is according to the clinical adult human daily prescription amount: (185 g raw herbs/60 kg body weigh) × 12.33 × extract yield (20%). The final extract was prepared for the low- and high-dosage groups at concentrations of 7.6 and 15.2 g/kg, respectively. This powder was dissolved in water to form two oral LQZ solutions for mice, at concentrations of 0.76 and 1.52 g/mL, and stored at −4 °C. Among them, a 0.76 g/mL LQZ solution will be used for UPLC-MS/MS detection.

For the preparation of LQZ serum samples, Initially, 8-week-old female BALB/c mice were selected and fasted for 12 h before sample collection, although they had access to water during the experiment. Mice received oral administration of 0.2 mL of the extract (7.6 g/kg). An hour later, the mice were anesthetized, and blood was collected from the retro-orbital venous plexus.[47] This blood was then placed in anticoagulant-free tubes and allowed to clot at room temperature for 1 h. Following this, it was centrifuged at 3000 rpm for 15 min. The supernatant obtained after centrifugation was transferred to new sterile centrifuge tubes. Subsequently, the serum samples were stored at −80 °C. These samples were then used for the identification of LQZ metabolites in serum via UPLC-MS/MS analysis.[48]

5.2. UPLC-ESI-MS/MS for LQZ Serum and Solution Component Analysis. *5.2.1. Sample Preparation and Extraction.* To prepare the samples, we removed them from the −80 °C freezer and thawed them on ice. We then Vortex each sample for 10 s to ensure thorough mixing. To minimize individual variations among the experimental mice, we combined all serum samples into a single composite sample. Additionally, a 0.76 g/mL LQZ solution sample was prepared for UPLC-MS/MS identification. We pipette 50 μL of each sample into a 1.5 mL centrifuge tube, and then 300 μL of 70% methanol containing the internal standard extraction solution. The mixture was vortexed at 12,000 rpm for 3 min at 4 °C and centrifuged for 10 min. Then, 200 μL of the supernatant was transferred to a new 1.5 mL centrifuge tube and let it stand at −20 °C for 30 min. Then, it was centrifuged again at 12,000 rpm for 3 min at 4 °C. Finally, 180 μL of the clear supernatant was transferred into an injection vial for LC-MS/MS detection.

5.2.2. UPLC Conditions. Sample extracts were analyzed using a UPLC-ESI-MS/MS system (UPLC, ExionLC AD, https://sciex.com.cn/) and a tandem mass spectrometry system (https://sciex.com.cn/). The UPLC conditions were set as follows: The column used was an Agilent SB-C18 (1.8 μm, 2.1 mm × 100 mm). The mobile phase consisted of solvents A (pure water with 0.1% formic acid) and B (acetonitrile with 0.1% formic acid). The sample analysis was conducted using a gradient program that started with 95% A and 5% B. Within 9 min, the program linearly shifted to 5% A and 95% B, maintaining this composition for 1 min, then returning to 95% A and 5% B over 1.1 min and maintaining for 2.9 min. The flow rate was 0.35 mL/min, the column oven temperature was 40 °C, and the injection volume was 2 μL. The effluent was alternately connected to an ESI-triple quadrupole-linear ion trap (QTRAP) MS.

5.2.3. ESI-Q TRAP-MS/MS. The ESI source operation parameters were set as follows: source temperature at 500 °C; ion spray voltage (IS) at 5500 V for positive ion mode and −4500 V for negative ion mode; ion source gases I and II (GSI and GSII) and curtain gas (CUR) at 50, 60, and 25 psi, respectively; and collision-activated dissociation (CAD) at high. QQQ scans were performed as MRM experiments with the collision gas (nitrogen) set to medium. Declustering potential (DP) and collision energy (CE) for individual MRM transitions were optimized. A specific set of MRM transitions was monitored for each period, corresponding to the elution of the metabolites within that period.

5.2.4. Data Analysis. Subsequently, substance identification was conducted based on our in-house metware database (MWDB) using secondary spectrum information. During the analysis, isotope signals and repetitive signals of K^+ ions, Na^+ ions, and NH_4^+ ions were excluded as well as repetitive signals of fragment ions originating from other larger molecular substances. Metabolite quantification was performed utilizing the multiple reaction monitoring (MRM) mode of a triple quadrupole mass spectrometer. This mode allowed the selection of characteristic ions for each substance, and the signal intensity (CPS) of these characteristic ions was obtained in the detector. Following this, the MultiQuant software was used to open the mass spectrometry files generated from the samples, and chromatographic peak integration and calibration were conducted. The peak area (Area) of each chromatographic peak represented the relative content of the corresponding substance. Finally, all integrated peak area data were exported and saved.

5.3. Network Construction and Analysis. First of all, based on the identified capable ingredients of LQZ, we get the biological targets from SwissTargetPrediction (www.swisstargetprediction.ch/), a Web site dedicated to the prediction of biological active small molecular targets in humans and other vertebrates. Meanwhile, we obtained AD putative targets from GeneCards (https://www.genecards.org/).[49] Subsequently, a venn diagram of gene symbols was generated by intersecting the LQZ targets and AD-associated targets. Then, the PPI network was constructed using STRING database v11.0 (www.string-db.org/) for retrieving interacting genes/proteins.[50] Finally, the result of the PPI network was exported and analyzed in Cytoscape v3.7.2 (www.cytoscape.org/) to determine the underlying mechanism of LQZ on AD.[51] We calculated the topological importance of nodes in the PPI network by determining their "Betweenness Centrality," "Closeness Centrality," and "Degree" parameters.

5.4. Analyses of Pathway Enrichment. To perform Gene Ontology (GO) enrichment and Kyoto Encyclopedia of Genes and Genomes (KEGG) pathway enrichment,[52] we input the potential overlapping targets into the DAVID database (https://david.ncifcrf.gov/summary.jsp). A threshold of $p < 0.05$ was used to determine the statistical significance in GO terms and KEGG pathways.

5.5. DNCB-Induced Atopic Dermatitis and Drug Treatment. In Figure 6A, an experimental plan for a DNCB-induced atopic dermatitis-like mouse model was presented. Eight-week-old female BALB/c mice, weight 20 ± 2 g, were sourced from Beijing Sibeifu Biotechnology Co. (Beijing, China) and received an Animal License of SXYK (Jing) 2019-0010. The Ethics Committee of Beijing University of Chinese Medicine (BUCM-4-2023020705-1092) granted approval for the animal procedures. After a week of

acclimation, the mice were evenly divided into five groups: the control group,-model group (DNCB group), Prednisolone treatment group (Pred group, 8 mg/kg), low-dose LQZ treatment group (LQZ-L group, 7.6 g/kg), and high-dose LQZ treatment group (LQZ-H group, 15.2 g/kg). Prednisolone was purchased from Tianjin Tianyao Pharmaceutical Co., Ltd. (Tianjin, China). Before the experiment (Day 0), DNCB (Chengdu Huaxia Chemical Reagent Co., Ltd., Chengdu, China) was dissolved in acetone and olive oil (3:1 v/v), the mice were anesthetized, and the back hair was removed. From Day 1 to Day 4, the mice's dorsal skin was sensitized with 150 μL of 2% DNCB every day and then again every 3 days, excluding the control group that was given acetone and olive oil topically in a 3:1 v/v ratio. This was the initial stage of allergic atopic dermatitis. In the second stage (Day 9−21), atopic dermatitis was reinduced. In the four experimental groups, we applied 150 μL of 0.5% DNCB evenly every other day on the dorsal skin as well as 20 μL of 0.5% DNCB specifically on the right ear to assess its effects in different areas. On the following day, we conducted tests and recorded various parameters related to the experiment. These included measuring the skin's physiological values, evaluating changes in ear thickness, and capturing images for documentation purposes.

From day 9 to day 22 of the experiment, mice in the treatment groups were administered oral treatments daily for 14 consecutive days at a dosage of 0.2 mL per day. The treatment groups included: the Prednisolone treatment group (Pred group, 8 mg/kg), low-dose LQZ treatment group (LQZ-L group, 7.6 g/kg), and high-dose LQZ treatment group (LQZ-H group, 15.2 g/kg). In contrast, the control group and DNCB group were given an equivalent volume of normal saline via gavage. On day 23, all mice were euthanized, and their dorsal skin, right ear tissue, blood, and spleen were collected for further analysis.

5.6. Histopathological Examination. The dorsal skin and right ears, fixed with paraformaldehyde, were embedded in paraffin and sliced into 5 μm sections using a microtome (Leica RM2016, America). These sections were then stained with either hematoxylin and eosin (H&E) or toluidine blue (TB) (China Pharmaceutical Group Co., Beijing, China). Histological analysis was then conducted by using an optical microscope to observe and evaluate general tissue features and mast cell infiltration of the sections.

5.7. Calculation of Spleen Coefficient and Evaluation of Dermatitis. The spleen coefficient, which is defined as the ratio of spleen tissue weight to body weight, was employed to estimate the severity of splenic injury. The severity of dermatitis was evaluated and recorded every other day in mouse lesions based on the presence of erythema/hemorrhage, edema, excoriation/erosion, and scaling/dryness. Dermatitis scores were calculated by summing the scores for each sign with the following criteria: no symptoms (score 0), moderate symptoms (score 2), and severe symptoms (score 3). Additionally, the thickness of the right ears in all mice was measured at the same time by using a micrometer.

5.8. Western Immunoblot Analysis. The total proteins were extracted from the dorsal skin tissue of mice using a RIPA lysis buffer at a ratio of 20 mg to 250 μL (supplemented with a protease/phosphatase inhibitor cocktail; Shanghai Epizyme Biomedical Technology Co., Ltd., Shanghai, China). Subsequently, the protein concentration was assessed using a BCA protein quantification kit following the instructions provided

by Shanghai Epizyme Biomedical Technology Co., Ltd., Shanghai, China. The lysates were mixed with 7.5% PAGE Gel (Shanghai Epizyme Biomedical Technology Co., Ltd., Shanghai, China), and then electrophoresis was performed. The extracted proteins were transferred to polyvinylidene fluoride membranes and blocked by Protein Free Rapid Blocking Buffer (Shanghai Epizyme Biomedical Technology Co., Ltd., Shanghai, China) for 15 min at room temperature, followed by overnight incubation with the primary antibody EGFR (1:5000, dilution), p-MAPK14 (1:500, dilution), p-MAPK1/3, MAPK1/3, and MAPK14 (1:1000 dilution), and GAPDH (1:10,000, dilution, all from Abways, Shanghai, China) at 4 °C. Afterward, the blots were incubated with secondary antibodies (1:5000 dilution, Abways, Shanghai, China) for an hour at room temperature. The manufacturer's instructions were followed to visualize the protein bands using an electrochemiluminescence (ECL) reagent (Shanghai Epizyme Biomedical Technology Co., Ltd., Shanghai, China), and protein expression was analyzed using ImageLab software.

5.9. Enzyme-Linked Immunosorbent Assay (ELISA). The levels of IL-1β, IL-6, and TNF-α in the serum samples were measured using ELISA kits (Jiangsu Meibiao Biotechnology Co., Ltd., Jiangsu, China) according to the manufacturer's instructions.

5.10. Statistical Analysis. The data were analyzed using one-way analysis of variance (ANOVA), and the results were presented as the mean $\pm$ standard deviation. A p-value of less than 0.05 was deemed to be significant.

■ ASSOCIATED CONTENT

Data Availability Statement

All data generated during this study are included in the manuscript and Supporting Files and are publicly available.

Ⓢ Supporting Information

The Supporting Information is available free of charge at https://pubs.acs.org/doi/10.1021/acsomega.3c09218.

Identified solution compounds of LQZ by UPLC-MS/MS (Table S1); identified serum compounds of LQZ by UPLC-MS/MS (Table S2); targets of LQZ (Table S3); targets of AD (Table S4); key targets of LQZ in AD (Table S5); total ion chromatogram monitored in negative and positive ion modes for LQZ serum and LQZ solution (Figure S1); potential overlapping targets between LQZ and AD (Figure S2); PPI network of related targets for LQZ in the treatment of AD (Figure S3); Go analyses and KEGG enrichment (Figure S4); compound−target−pathway network (Figure S5); effects of LQZ on the spleen coefficient, dermatitis scores, and ear thickness (Figure S6); effects of LQZ on histopathologic findings (Figure S7); LQZ decreases the level of IL-1β, IL-6, and TNF-α in a serum (Figure S8); LQZ inhibits protein expressions of EGFR, p-MAPK1/3, and p-MAPK14 in AD mice (Figure S9); and modulating the MAPK signaling pathway of LQZ against AD (Figure S10) (PDF)

■ AUTHOR INFORMATION

Corresponding Author

Zhanxue Sun − *Beijing University of Chinese Medicine Affiliated Third Hospital, Beijing 100029, China;* Email: sunzhanxue@163.com

Authors

Lili Zhang − *Beijing University of Chinese Medicine Affiliated Third Hospital, Beijing 100029, China;* ⊙ orcid.org/0000-0002-6906-8893

Huili Zhang − *Beijing University of Chinese Medicine Dongfang Hospital, Beijing 100078, China*

Xiaoyu Niu − *Beijing University of Chinese Medicine Affiliated Third Hospital, Beijing 100029, China*

Xuan Zhang − *Beijing University of Chinese Medicine Affiliated Third Hospital, Beijing 100029, China*

Xingtong Chen − *Beijing University of Chinese Medicine Affiliated Third Hospital, Beijing 100029, China*

Shengyi Lei − *Beijing University of Chinese Medicine Affiliated Third Hospital, Beijing 100029, China*

Shengnan Ma − *Beijing University of Chinese Medicine Affiliated Third Hospital, Beijing 100029, China*

Complete contact information is available at:
https://pubs.acs.org/10.1021/acsomega.3c09218

Author Contributions

§L.Z. and H.Z. contributed equally to this work. Z.S. and L.Z. conceived and designed the experiments. H.Z. and X.N. performed the experiments. X.Z., X.C., S.L., and S.M. analyzed the data. L.Z. wrote the manuscript. All authors approved on the final submitted version of the manuscript.

Notes

The authors declare no competing financial interest.

Ethics Statement The experimental protocols were approved by Beijing University of Traditional Chinese Medicine, and the certificate number is BUCM-4-2023020705-1092.

■ ABBREVIATIONS

LQZ	Liangxue-Qushi-Zhiyang decoction
AD	atopic dermatitis
UPLC-ESI-MS/MS	ultra-performance liquid chromatography-electrospray ionization-tandem mass spectrometry
DNCB	2,4-dinitrochlorobenzene
TH2 cells	type 2 skin lymphocytes
TCM	traditional Chinese medicine
GO	gene ontology
KEGG	Kyoto encyclopedia of genes and genomes
H&E	hematoxylin and eosin
TB	toluidine blue
ELISA	enzyme-linked immunosorbent assay
Pred group	prednisolone group
DNCB group	model group
LQZ-L group	low-dose LQZ treatment group
LQZ-H group	high-dose LQZ treatment group

■ REFERENCES

(1) Ständer, S. Atopic Dermatitis. *N. Engl. J. Med.* **2021**, *384* (12), 1136−1143.

(2) Barbarot, S.; Auziere, S.; Gadkari, A.; Girolomoni, G.; Puig, L.; Simpson, E. L.; Margolis, D. J.; de Bruin-Weller, M.; Eckert, L. Epidemiology of atopic dermatitis in adults: Results from an international survey. *Allergy* **2018**, *73* (6), 1284−1293.

(3) Weidinger, S.; Beck, L. A.; Bieber, T.; Kabashima, K.; Irvine, A. D. Atopic dermatitis. *Nat. Rev. Dis. Primers* **2018**, *4* (1), No. 1.

(4) Ramirez, F. D.; Chen, S.; Langan, S. M.; Prather, A. A.; McCulloch, C. E.; Kidd, S. A.; Cabana, M. D.; Chren, M. M.; Abuabara, K. Association of Atopic Dermatitis With Sleep Quality in Children. *JAMA Pediatr.* **2019**, *173* (5), No. e190025.

(5) Traidl, S.; Roesner, L.; Zeitvogel, J.; Werfel, T. Eczema herpeticum in atopic dermatitis. *Allergy* **2021**, *76* (10), 3017−3027.

(6) Sroka-Tomaszewska, J.; Trzeciak, M. Molecular Mechanisms of Atopic Dermatitis Pathogenesis. *Int. J. Mol. Sci.* **2021**, *22* (8), No. 4130. DOI: 10.3390/ijms22084130.

(7) Guttman-Yassky, E.; Waldman, A.; Ahluwalia, J.; Ong, P. Y.; Eichenfield, L. F. Atopic dermatitis: pathogenesis. *Semin. Cutaneous Med. Surg.* **2017**, *36* (3), 100−103.

(8) Langan, S. M.; Irvine, A. D.; Weidinger, S. Atopic dermatitis. *Lancet* **2020**, *396* (10247), 345−360.

(9) Wollenberg, A.; Oranje, A.; Deleuran, M.; Simon, D.; Szalai, Z.; Kunz, B.; Svensson, A.; Barbarot, S.; von Kobyletzki, L.; Taieb, A.; de Bruin-Weller, M.; Werfel, T.; Trzeciak, M.; Vestergard, C.; Ring, J.; Darsow, U. ETFAD/EADV Eczema task force 2015 position paper on diagnosis and treatment of atopic dermatitis in adult and paediatric patients. *J. Eur. Acad. Dermatol. Venereol.* **2016**, *30* (5), 729−747.

(10) Barnes, L.; Kaya, G.; Rollason, V. Topical corticosteroid-induced skin atrophy: a comprehensive review. *Drug Saf.* **2015**, *38* (5), 493−509.

(11) Paller, A. S.; Tom, W. L.; Lebwohl, M. G.; Blumenthal, R. L.; Boguniewicz, M.; Call, R. S.; Eichenfield, L. F.; Forsha, D. W.; Rees, W. C.; Simpson, E. L.; Spellman, M. C.; Gold, L. F. S.; Zaenglein, A. L.; Hughes, M. H.; Zane, L. T.; Hebert, A. A. Efficacy and safety of crisaborole ointment, a novel, nonsteroidal phosphodiesterase 4 (PDE4) inhibitor for the topical treatment of atopic dermatitis (AD) in children and adults. *J. Am. Acad. Dermatol.* **2016**, *75* (3), 494−503.e6.

(12) Huang, M.; Hua, N.; Zhuang, S.; Fang, Q.; Shang, J.; Wang, Z.; Tao, X.; Niu, J.; Li, X.; Yu, P.; Yang, W. Cux1(+) proliferative basal cells promote epidermal hyperplasia in chronic dry skin disease identified by single-cell RNA transcriptomics. *J. Pharm. Anal.* **2023**, *13* (7), 745−759.

(13) Newsom, M.; Bashyam, A. M.; Balogh, E. A.; Feldman, S. R.; Strowd, L. C. New and Emerging Systemic Treatments for Atopic Dermatitis. *Drugs* **2020**, *80* (11), 1041−1052.

(14) Goh, M. S.; Yun, J. S.; Su, J. C. Management of atopic dermatitis: a narrative review. *Med. J. Aust.* **2022**, *216* (11), 587−593.

(15) Sun, Z.; Wang, J.; Wang, X. Effect of Liangxue Qushi Zhiyang Decoction on IL-17A and IL-23 in Patients with Atopic Dermatitis of Blood heat and Dampness Accumulation Syndrome. *Chin. J. Tradit. Chin. Med.* **2021**, *36* (09), 5653−5656.

(16) Sun, Z. Effect of Liangxuequshizhiyang Decoction on the Concentration of Serum IL-2 and IL-4 and Leukotriene B4 of Lesions in Mice Model with Atopic Dermatitis. *Chin. J. Dermatovenereol.* **2016**, *30* (11), 1169−1171.

(17) Yang, R. J.; Zou, J.; Liu, J. Y.; Dai, J. K.; Wan, J. B. Click chemistry-based enrichment strategy for tracing cellular fatty acid metabolism by LC-MS/MS. *J. Pharm. Anal.* **2023**, *13* (10), 1221−1231.

(18) Zhang, L.; Li, Y.; Tang, F.; Liu, D.; Zhao, X. L.; Zhang, J. N.; Xia, J.; Wu, J. J.; Yang, Y.; Peng, C.; Ao, H. New perspectives on the therapeutic potential of quercetin in non-communicable diseases: Targeting Nrf2 to counteract oxidative stress and inflammation *J. Pharm. Anal.* **2023**, DOI: 10.1016/j.jpha.2023.12.020.

(19) Huang, P.; Hu, F.; Yang, Z. B.; Pan, Y.; Zhou, R.; Yan, Y. N.; Wang, H. Z.; Wang, C. Matrine regulates Th1/Th2 inflammatory

responses by inhibiting the Hsp90/NF-κB signaling axis to alleviate atopic dermatitis. *Kaohsiung J. Med. Sci.* **2023**, *39* (5), 501−510.

(20) Dong, L.; Yin, L.; Zhang, Y.; Fu, X.; Lu, J. Anti-inflammatory effects of ononin on lipopolysaccharide-stimulated RAW 264.7 cells. *Mol. Immunol.* **2017**, *83*, 46−51.

(21) Nogales, C.; Mamdouh, Z. M.; List, M.; Kiel, C.; Casas, A. I.; Schmidt, H. Network pharmacology: curing causal mechanisms instead of treating symptoms. *Trends Pharmacol. Sci.* **2022**, *43* (2), 136−150.

(22) Hopkins, A. L. Network pharmacology: the next paradigm in drug discovery. *Nat. Chem. Biol.* **2008**, *4* (11), 682−690.

(23) Li, S.; Zhang, B. Traditional Chinese medicine network pharmacology: theory, methodology and application. *Chin. J. Nat. Med.* **2013**, *11* (2), 110−120.

(24) Wang, H.; Wu, R.; Xie, D.; Ding, L.; Lv, X.; Bian, Y.; Chen, X.; Nisma Lena, B. A.; Wang, S.; Li, K.; Chen, W.; Ye, G.; Sun, M. A Combined Phytochemistry and Network Pharmacology Approach to Reveal the Effective Substances and Mechanisms of Wei-Fu-Chun Tablet in the Treatment of Precancerous Lesions of Gastric Cancer. *Front. Pharmacol.* **2020**, *11*, No. 558471.

(25) Tan, Y.; Huang, Z.; Liu, X.; Li, X.; Stalin, A.; Fan, X.; Wu, Z.; Wu, C.; Lu, S.; Zhang, F.; Chen, M.; Huang, J.; Cheng, G.; Li, B.; Guo, S.; Yang, Y.; Zhang, S.; Wu, J. Integrated serum pharmacochemistry, 16S rRNA sequencing and metabolomics to reveal the material basis and mechanism of Yinzhihuang granule against non-alcoholic fatty liver disease. *J. Ethnopharmacol.* **2023**, *310*, No. 116418.

(26) Walczak, H. TNF and ubiquitin at the crossroads of gene activation, cell death, inflammation, and cancer. *Immunol. Rev.* **2011**, *244* (1), 9−28.

(27) Liang, X.; Huang, Y.; Pan, X.; Hao, Y.; Chen, X.; Jiang, H.; Li, J.; Zhou, B.; Yang, Z. Erucic acid from Isatis indigotica Fort. suppresses influenza A virus replication and inflammation in vitro and in vivo through modulation of NF-κB and p38 MAPK pathway. *J. Pharm. Anal.* **2020**, *10* (2), 130−146.

(28) Williams, H. C.; Chalmers, J. Prevention of Atopic Dermatitis. *Acta Derm.-Venereol.* **2020**, *100* (12), 380−388.

(29) Hanusch, B.; Sinningen, K.; Brinkmann, F.; Dillenhöfer, S.; Frank, M.; Jöckel, K. H.; Koerner-Rettberg, C.; Holtmann, M.; Legenbauer, T.; Langrock, C.; Reinehr, T.; Maasjosthusmann, P.; Beckmann, B.; Hamelmann, E.; Tsikas, D.; Lücke, T. Characterization of the L-Arginine/Nitric Oxide Pathway and Oxidative Stress in Pediatric Patients with Atopic Diseases. *Int. J. Mol. Sci.* **2022**, *23* (4), No. 2136, DOI: 10.3390/ijms23042136.

(30) Liang, M.; Wang, Z.; Li, H.; Liu, B.; Yang, L. l-Arginine prevents 4-hydroxy-2-nonenal accumulation and depresses inflammation via inhibiting NF-κB activation. *J. Biochem. Mol. Toxicol.* **2022**, *36* (8), No. e23087.

(31) Wang, J.; Li, H.; Yang, Z.; Huang, C.; Sun, Y.; Hu, X. Elucidation of the Mechanisms and Molecular Targets of Run-zao-zhiyang Capsule for Itch based on Network Pharmacology, Molecular Docking and In Vitro Experiment. *Comb. Chem. High Throughput Screening* **2023**, *26* (10), 1866−1878.

(32) Zhang, Q.; Chen, S.; Guo, Y.; He, F.; Fu, J.; Ren, W. Phenylalanine diminishes M1 macrophage inflammation. *Sci. China Life Sci.* **2023**, *66*, 2862−2876, DOI: 10.1007/s11427-022-2296-0.

(33) Johnson, G. H.; Fritsche, K. Effect of dietary linoleic acid on markers of inflammation in healthy persons: a systematic review of randomized controlled trials. *J. Acad. Nutr. Diet.* **2012**, *112* (7), 1029−1041.e15.

(34) Su, H.; Liu, R.; Chang, M.; Huang, J.; Jin, Q.; Wang, X. Effect of dietary alpha-linolenic acid on blood inflammatory markers: a systematic review and meta-analysis of randomized controlled trials. *Eur. J. Nutr.* **2018**, *57* (3), 877−891.

(35) Xiong, X.; Huang, C.; Wang, F.; Dong, J.; Zhang, D.; Jiang, J.; Feng, Y.; Wu, B.; Xie, T.; Cheng, L. Qingxue jiedu formulation ameliorated DNFB-induced atopic dermatitis by inhibiting STAT3/MAPK/NF-κB signaling pathways. *J. Ethnopharmacol.* **2021**, *270*, No. 113773.

(36) Edslev, S. M.; Agner, T.; Andersen, P. S. Skin Microbiome in Atopic Dermatitis. *Acta Derm.-Venereol.* **2020**, *100* (12), 358−366.

(37) Drosten, M.; Barbacid, M. Targeting the MAPK Pathway in KRAS-Driven Tumors. *Cancer Cell* **2020**, *37* (4), 543−550.

(38) Yeung, Y. T.; Aziz, F.; Guerrero-Castilla, A.; Arguelles, S. Signaling Pathways in Inflammation and Anti-inflammatory Therapies. *Curr. Pharm. Des.* **2018**, *24* (14), 1449−1484.

(39) Xia, T.; Liang, X.; Liu, C. S.; Hu, Y. N.; Luo, Z. Y.; Tan, X. M. Network Pharmacology Integrated with Transcriptomics Analysis Reveals Ermiao Wan Alleviates Atopic Dermatitis via Suppressing MAPK and Activating the EGFR/AKT Signaling. *Drug Des., Dev. Ther.* **2022**, *16*, 4325−4341.

(40) Liu, J.; Tao, Y.; Zou, X.; Liu, Q.; Meng, X.; Zhang, Y.; Su, J. In vitro and in vivo exploration of the anti-atopic dermatitis mechanism of action of Tibetan medicine Qi-Sai-Er-Sang-Dang-Song decoction. *J. Ethnopharmacol.* **2023**, *306*, No. 116155.

(41) Meng, Y.; Liu, Z.; Zhai, C.; Di, T.; Zhang, L.; Zhang, L.; Xie, X.; Lin, Y.; Wang, N.; Zhao, J.; Wang, Y.; Li, P. Paeonol inhibits the development of 1-chloro-2,4-dinitrobenzene-induced atopic dermatitis via mast and T cells in BALB/c mice. *Mol. Med. Rep.* **2019**, *19* (4), 3217−3229.

(42) Ngo, H. T. T.; Fang, M.; Hwang, E.; Kim, Y.; Park, B.; Seo, S. A.; Do, N. Q.; Nguyen, Q. T. N.; Yi, T. H. Inhibitory Effects of Urtica thunbergiana Ethanol Extract on Atopic Dermatitis-Induced NC/Nga Mice. *Antioxidants* **2020**, *9* (3), No. 197, DOI: 10.3390/antiox9030197.

(43) Tsai, Y. C.; Chang, H. H.; Chou, S. C.; Chu, T. W.; Hsu, Y. J.; Hsiao, C. Y.; Lo, Y. H.; Wu, N. L.; Chang, D. C.; Hung, C. F. Evaluation of the Anti-Atopic Dermatitis Effects of α-Boswellic Acid on Tnf-α/Ifn-γ-Stimulated HaCat Cells and DNCB-Induced BALB/c Mice. *Int. J. Mol. Sci.* **2022**, *23* (17), No. 9863, DOI: 10.3390/ijms23179863.

(44) Demchenko, Y. N.; Glebov, O. K.; Zingone, A.; Keats, J. J.; Bergsagel, P. L.; Kuehl, W. M. Classical and/or alternative NF-kappaB pathway activation in multiple myeloma. *Blood* **2010**, *115* (17), 3541−3552.

(45) Boothe, W. D.; Tarbox, J. A.; Tarbox, M. B. Atopic Dermatitis: Pathophysiology. *Adv. Exp. Med. Biol.* **2017**, *1027*, 21−37.

(46) Weidinger, S.; Novak, N. Atopic dermatitis. *Lancet* **2016**, *387* (10023), 1109−1122.

(47) Li, Q.; Jia, C.; Wu, H.; Liao, Y.; Yang, K.; Li, S.; Zhang, J.; Wang, J.; Li, G.; Guan, F.; Leung, E.; Yuan, Z.; Hua, Q.; Pan, R. Y. Nao Tan Qing ameliorates Alzheimer's disease-like pathology by regulating glycolipid metabolism and neuroinflammation: A network pharmacology analysis and biological validation. *Pharmacol. Res.* **2022**, *185*, No. 106489.

(48) Fraga, C. G.; Clowers, B. H.; Moore, R. J.; Zink, E. M. Signature-discovery approach for sample matching of a nerve-agent precursor using liquid chromatography-mass spectrometry, XCMS, and chemometrics. *Anal. Chem.* **2010**, *82* (10), 4165−4173.

(49) Stelzer, G.; Rosen, N.; Plaschkes, I.; Zimmerman, S.; Twik, M.; Fishilevich, S.; Stein, T. I.; Nudel, R.; Lieder, I.; Mazor, Y.; Kaplan, S.; Dahary, D.; Warshawsky, D.; Guan-Golan, Y.; Kohn, A.; Rappaport, N.; Safran, M.; Lancet, D. The GeneCards Suite: From Gene Data Mining to Disease Genome Sequence Analyses. *Curr. Protoc. Bioinf.* **2016**, *54*, 1−30.

(50) Szklarczyk, D.; Gable, A. L.; Lyon, D.; Junge, A.; Wyder, S.; Huerta-Cepas, J.; Simonovic, M.; Doncheva, N. T.; Morris, J. H.; Bork, P.; Jensen, L. J.; Mering, C. V. STRING v11: protein-protein association networks with increased coverage, supporting functional discovery in genome-wide experimental datasets. *Nucleic Acids Res.* **2019**, *47* (D1), D607−D613.

(51) Shannon, P.; Markiel, A.; Ozier, O.; Baliga, N. S.; Wang, J. T.; Ramage, D.; Amin, N.; Schwikowski, B.; Ideker, T. Cytoscape: a software environment for integrated models of biomolecular interaction networks. *Genome Res.* **2003**, *13* (11), 2498−2504.

(52) Huang, D. W.; Sherman, B. T.; Lempicki, R. A. Systematic and integrative analysis of large gene lists using DAVID bioinformatics resources. *Nat. Protoc.* **2009**, *4* (1), 44−57.